Source Process of the 1974 and 1975 Earthquakes in Kurile Islands in Special Relation to the Difference in Excitation of Tsunami

Sci. Rep. Tôhoku Univ., Ser. 5, Geophysics, Vol. 24, No. 4, pp. 113–132, 1977.

Source Process of the 1974 and 1975 Earthquakes in Kurile Islands in Special Relation to the Difference in Excitation of Tsunami

MASAYUKI TAKEMURA, JUNJI KOYAMA* and ZIRO SUZUKI

Geophysical Institute, Faculty of Science
Tôhoku University, Sendai 980, Japan

(Received October 5, 1977)

Abstract: Three earthquakes in southern Kurile region in 1974 and 1975 are studied especially in relation to the difference in excitation of tsunami. The shock on June 10, 1975 was accompanied with an anomalously large tsunami compared with the other two although the difference in magnitude is not so much. The three events are concluded to have the similar thrust type mechanisms, based on long period P, S and Rayleigh waves. The dip angle of the fault plane of above mentioned earthquake on June 10 is smallest among the three and this is compatible with the plate tectonics because its epicenter is closest to trench. The effective seismic moment of this event is almost the same as the others in the period range around 30 sec, while that in the range around 150 sec is much larger than the others. This implies that the earthquake has a longer rise time and it makes a good explanation for the strong excitation of tsunami in this case. Some other natures of these earthquakes are also discussed.

1. Introduction

Iida (1958) had made a statistical study on the relation between earthquake and tsunami magnitudes and he obtained the formula as

$$m = 2.61\,M - 18.44\,, \tag{1}$$

where the earthquake magnitude M is the value determined by JMA and the tsunami magnitude m is that in Imamura and Iida's scale (Iida, 1958). In some cases, however, this formula does not explain the observed data so well. Fig. 1 shows the comparison of the formula and observation for ten events in and near Japan. For example, the tsunami associated with the Sanriku Earthquake on Jun. 15, 1896 is much larger than expected by this formula.

A series of earthquakes of Sept. 27, 1974 (Ms =6.7), June 10, 1975 (Ms=7.0) and June 13. 1975 (Ms=6.4) took place recently in southern Kurile region. Ms is the surface wave magnitude determined by USGS. The last shock was the largest aftershock of the second one. These are called the 1974 earthquake, the main shock and the aftershock provisionally in this paper for convenience. Parameters of these events are tabulated in Table 1. The magnitudes of tsunamis of these shocks are much different. The 1974 earthquake generated a small tsunami and the main shock was accompanied by a big tsunami, whereas no observable tsunami was excited by the

* Now at Marine Science Institute, the University of Texas, Galveston, USA.

Table 1. The parameters of hypocenters reported by USGS and earthquake and tsunami magnitudes.

Date (G.M.T.)	Origin time	Lat.	Long.	Depth	M_b (GS)	Ms (GS)	M (JMA)	m*
JUN. 10, 1975	13h 47m 14.50s	43.024°N	147.734°E	15.2km	5.8	7.0	7.0	1.5
JUN. 13, 1975	18 08 11.70	43.489	147.709	18.6	6.1	6.4	6.5	—
SEP. 27, 1974	05 47 29.44	43.176	146.651	43.0	6.0	6.7	6.6	−1.0

*m: tsunami magnitude according to Hatori (1975)

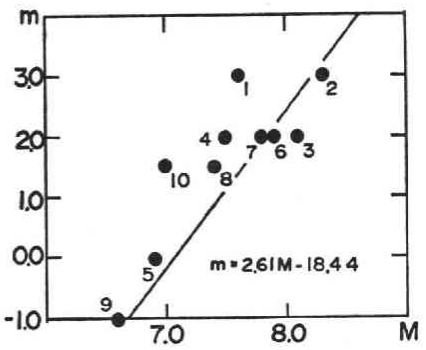

Fig. 1

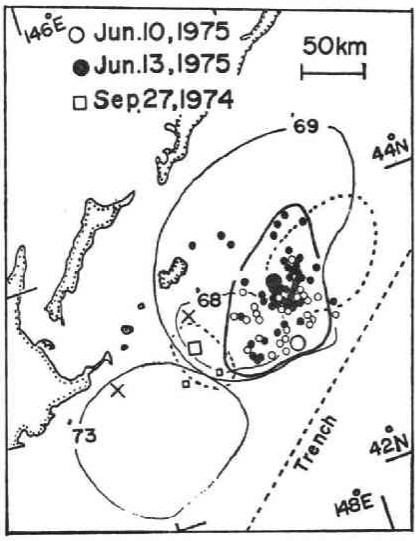

Fig. 2

Fig. 1 Relation between tsunami and earthquake magnitudes. Solid line corresponds to Eq. (1) by Iida. The numbered solid circles represent the observational data of Table 9.

Fig. 2 Epicenters of three earthquakes. Open and solid circles indicate aftershocks within one and ten days after the main shock on June 10, 1975 and open squares the aftershocks of the 1974 earthquake. Dotted curves are tsunami source regions for the main shock and the 1974 earthquake. Crosses show epicenters of major earthquakes in this region before 1974 and solid curves are their aftershock areas.

aftershock. As seen in Fig. 1, the main shock was associated with an anormalously large tsunami in comparison to its earthquake magnitude. This series, therefore, gives an example of the above mentioned discrepancy between the formula (1) and observation. This study aims at the elucidation of cause of this discrepancy based on the differences in source mechanisms and source spectra of the three events.

2. Description of the earthquakes

Epicenters of the three events of the 1974 earthquake, the main shock and the largest aftershock are shown in Fig. 2 by different symbols explained in the figure. Epicenters of other aftershocks are also given in this figure, where open and solid circles stand for the aftershocks within one and ten days after the main shock respectively.

These locations refer to USGS. Dashed curves indicate the tsunami source regions for the 1974 earthquake and the main shock according to Hatori (1975). Since the largest aftershock was not accompanied with tsunami of observable size, the source region cannot be shown.

Major earthquakes before the series in this region were those on Jan. 29, 1968, Aug. 11, 1969 and June 17, 1973. Crosses in Fig. 2 respresent the epicenters of major shocks in 1968 and 1973. The earthquake in 1969 was associated with many precursory shocks and the accuracy of location of epicenter is very poor. Hence the epicenter of this shock is excluded from the figure. The aftershock areas of these three major earthquakes are shown by thin solid curves based on the report by ISC.

Fig. 2 indicates that the aftershock area of the main shock is included in that of the 1969 event. The epicenter was located near the trenchward edge of the aftershock area. Kelleher *et al.* (1973) stated that the epicenter of major earthquake near trench is usually situated on the island arc side of aftershock area and the rupture proceeds from island to trench, examples being seen in the cases of the 1968 and 1973 earthquakes. The present main shock, therefore, has a contrary feature to that in usual cases.

The epicenter of the 1974 event was located at the boundary of aftershock areas of the 1968 and 1973 earthquakes. The number of aftershocks of this event was very few.

The long period seismograms of the three events at KEV of WWSSN are reproduced in Fig. 3. This figure shows that the main shock has several different features from other two cases. The initial P wave train is very complex in its form, long in duration and large in amplitude. The later part of the train with large amplitude cannot be attributed to such phases as PP, PcP, PPP and PcS, as is clear in Fig. 3. A discussion about this point will be made in a later section.

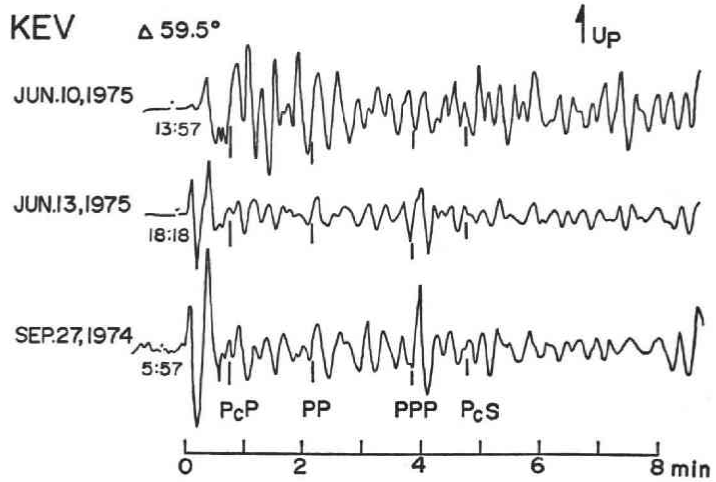

Fig. 3 Seismograms in vertical component of the three earthquakes at KEV.

Fig. 4 SH seismograms of the main shock. Solid line indicates the onset of the precursory shock.

The initial wave train of the main shock begins with a small amplitude phase followed by large amplitude ones, which may correspond to the main fracture. This sort of small amplitude before large amplitude is found also at the beginning of S phase as seen in SH seismograms in Fig. 4, which shows three examples of them. This indicates the precursory foreshock activity immediately before the main fracture. The study of this foreshock will be made as well.

3. Source mechanism

Directions of initial P motions and polarization angles of S waves are read from the long period seismograms at WWSSN stations for the main fracture and precursory shock of the main shock, the aftershock and the 1974 earthquake. The polarization angles of S waves are listed in Tables 2, 3, and 4, respectively. Their mechanism solutions from polarization angles are determined by the method of least squares according to Hirasawa (1966). When the E-W and N-S components do not behave in phase, the determination is abandoned because of possible contamination of S wave with other phases. The solutions obtained are given in Figs. 5(a), 6(a), and 7(a) on the lower half of focal sphere in equal area projection.

Figs. 5(b), 6(b) and 7(b) show the directions of P wave initial motions as well as the same mechanisms as in Figs. 5(a), 6(a) and 7(a). These figures imply that the mechanism solution obtained from S waves is compatible with P wave data for every earthquake.

As mentioned in the previous section, a small precursory event took place about 10 sec before the main fracture in the event on June 10, 1975. The directions of initial P motions and polarization angles of S waves of this precursory shock are shown in Table 2 and Fig. 8. The mechanism of the main fracture is also shown in Fig. 8. Although the number of data for the precursory shock is too few to determine its mechanism from them, Fig. 8 shows that the mechanism of the precursor is similar to that of the main fracture.

The mechanism solution thus obtained clearly indicates thrust type faulting in every case. Numerical results for dip angles and dip directions of fault and auxiliary planes are given in Table 5 together with their standard deviations The identification of fault plane is based on the idea that the plane dipping towards island arc should be the fault plane according to the global tectonics. From Table 5 the dip angle of fault

Table 2. The S wave polarization angles of both the main fracture and the precursory shock of the main shock. Azimuth is an azimuth angle measured clockwise from the north. Inc. Ang. is an incident angle measured from the downward vertical.

Station	Inc. Ang.	Azimuth	Pol. Ang.	Pol. Ang. (Precursory)
ADE	19.9°	187.6°	129.9°	122.4°
ANP	31.4	238.8	88.7	
ATU	18.3	318.9	12.5	− 0.4
COL	28.0	35.6	−119.2	−129.5
COR	24.0	54.8	−114.5	−134.7
CTA	23.5	181.6	146.8	
GDH	22.6	7.9	− 58.4	− 68.9
HKC	29.6	244.2	99.7	
BKS	23.0	60.5	−105.3	
KON	21.4	339.1	− 16.0	
LEM	23.8	226.7	76.7	
NUR	22.6	333.2	− 16.5	
PMG	25.9	180.7	129.4	124.6
RIV	20.3	177.1	137.7	135.2
TAB	21.3	305.7	17.4	
VAL	18.6	346.5	− 33.2	
WES	17.5	27.9	− 87.8	

Table 3. The S wave polarization angles of the aftershock. The same notation as in Table 2 is adopted.

Station	Inc. Ang.	Azimuth	Pol. Ang.
ANP	31.3°	238.0°	94.7°
COL	28.1	35.9	−123.5
COP	20.9	335.5	− 83.5
COR	24.0	55.0	−126.6
CTA	23.4	181.5	123.5
GDH	22.8	8.1	− 82.7
HKC	29.8	243.5	89.9
KBS	25.3	350.5	− 96.3
KEV	24.4	339.6	− 92.7
KIP	26.4	98.2	−166.7
LEM	23.8	226.5	71.9
NUR	22.8	333.0	− 78.8
OGD	17.6	30.6	− 84.7
PMG	25.9	180.7	145.1
RIV	20.3	177.1	147.4
SNG	28.1	242.8	105.5
VAL	18.7	346.5	−103.4
WES	17.6	27.8	− 88.7

Table 4. The S wave polarization angles of the 1974 earthquake. The same notation as in Table 2 is adopted.

Station	Inc. Ang.	Azimuth	Pol. Ang.
AAE	19.6°	288.5°	4.2°
ADE	24.9	186.3	113.5
AFI	27.8	135.7	157.1
ALQ	25.0	53.3	−115.9
ATU	23.0	317.9	−101.4
BAG	37.7	227.0	119.2
BKS	28.5	59.8	−116.9
COL	35.4	35.7	−134.2
COP	26.1	334.8	−120.6
DAL	22.7	48.8	−119.5
ESK	24.8	342.7	−121.4
GDH	28.3	7.5	−114.7
HNR	32.1	163.1	141.2
JCT	22.7	52.3	−112.3
KBS	31.7	350.3	−123.2
KEV	30.7	339.2	−124.3
KON	26.9	338.4	−125.5
LEM	30.1	225.1	93.5
LON	29.9	51.5	−121.3
MSH	29.2	296.3	−105.6
PMG	32.6	178.8	145.9
TAB	27.0	304.8	−109.6

plane of the main shock is safely said to be smaller than those of the other two earthquakes by about ten degrees, taking the standard deviation in the table into consideration. Since the epicenter of the main shock is located farther off the island coast than the others, this fact is consistent with the idea of plate tectonics. The compatibility of

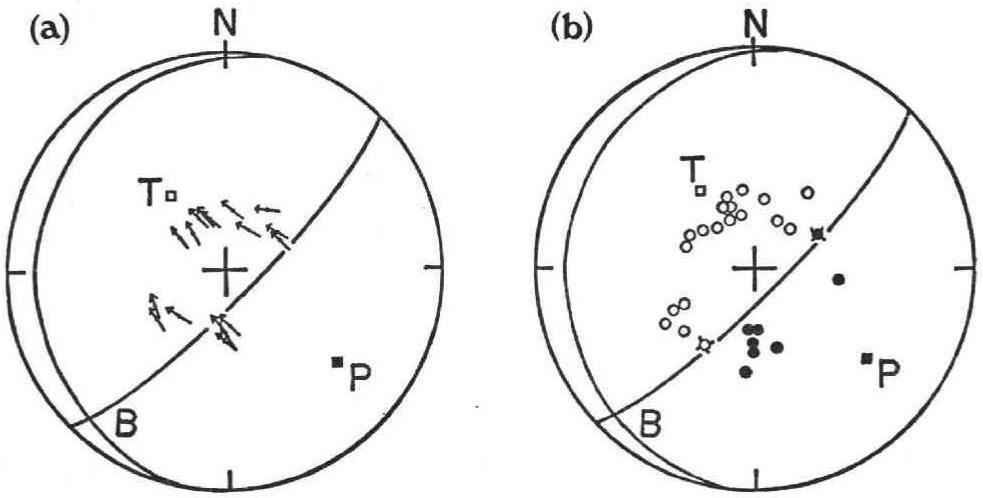

Fig. 5 Focal mechanism solution of the main fracture in the event on June 10, 1975. Data are projected on the lower half of focal sphere in equal area projection. Solid curves indicate the solution by least squares method from polarization angles of S waves in every figure. P, T and B mean pressure, tension and null axes respectively. (a) Polarization angles of S waves and the solution. (b) Directions of P wave initial motions and the solution from S waves. Open and solid circles show rarefaction and compression respectively and circles with crosses indicate the data judged to be near the nodal planes.

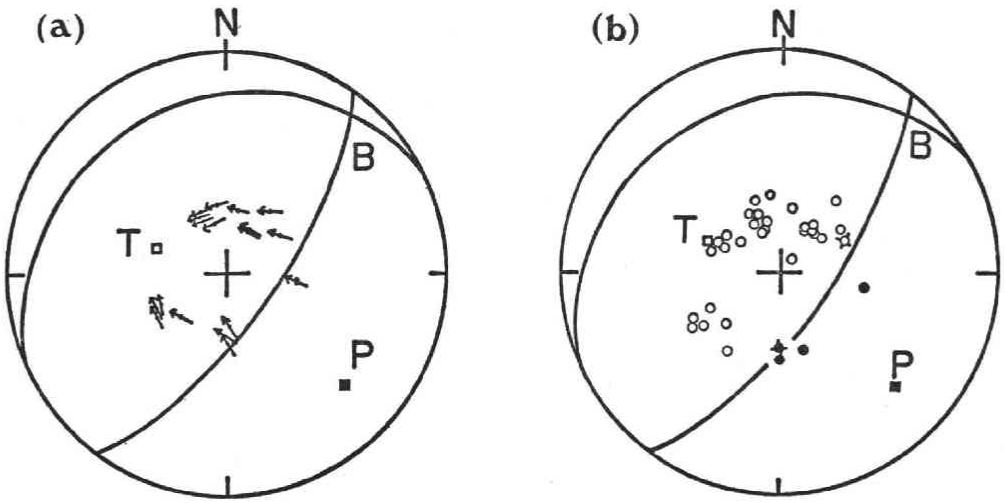

Fig. 6 Focal mechanism solution and data for the aftershock. The way of representation is the same as in Fig. 5. (a) S wave data and the solution from S waves. (b) P wave data and the solution from S waves.

these source mechanisms with the observed amplitudes of surface waves will be described in a later section.

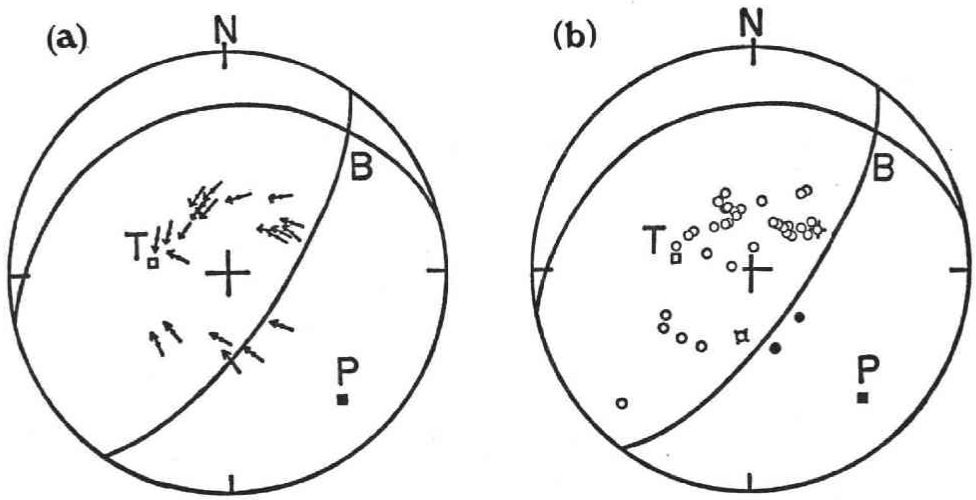

Fig. 7 Focal mechanism solution and data for the 1974 earthquake. The way of representation is the same as in Fig. 5. (a) S wave data and the solution from S waves. (b) P wave data and the solution from S waves.

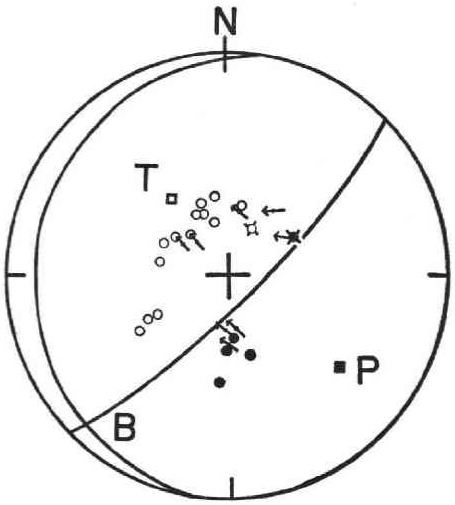

Fig. 8 Polarization angles and directions of P wave initial motions for the precursory shock of the main shock. The solution is that for the main fracture from S wave data. Notations and projection are the same as in Fig. 5.

Table 5. Numerical results of focal mechanism solutions from S waves.

Date (G.M.T.)	Fault plane		Auxiliary plane	
	Dip direction	Dip angle	Dip direction	Dip angle
JUN. 10,1975	−80.8° ±38.7°	12.7° ±5.8°	135.6° ±5.3°	79.7° ±3.5°
JUN. 13,1975	−24.3 ±21.8	21.0 ±2.8	125.9 ±7.0	71.6 ±1.7
SEP. 27,1974	−13.0 ± 7.3	26.2 ±2.0	124.8 ±3.7	69.9 ±0.7

4. Source spectrum and effective moment

Kanamori (1972) defined the effective moment as a seismic moment due to a virutal dislocation of step function at every frequency. Let $D(t)$ represent the source shear dislocation, where $D(t)=0$ for $t<0$ and $D(\infty)=Do$ which is the static dislocation. Then the moment function $M(t)$ for the equivalent point source of double couple is proportional to $D(t)$. If the amplitude spectral density of moment is denoted by $|\hat{M}(\omega)|$, the effective moment $M_e(\omega)$ is expressed as

$$M_e(\omega) = \omega |\hat{M}(\omega)| . \tag{2}$$

It is obvious that when $D(t)$ behaves as a step function of Heaviside type with respect to time or the angular frequency ω is zero, $M_e(\omega)$ coincides with the static seismic moment.

The effective moment $M_e(\omega)$ is represented in terms of body wave spectral amplitude $U_c(\omega)$ as

$$M_e(\omega) = \frac{4\pi\rho V_c^3}{R_{\theta\phi}{}^c\, G_c(\Delta, h)} \left| \frac{U_c(\omega)}{H_m{}^c(\omega)\cdot H_{cr}{}^c(\omega)\cdot H_i(\omega)} \right| , \tag{3}$$

where the subscript c stands for P or S wave, ρ and V_c represent density and wave velocity near the focal region respectively, and $R_{\theta\phi}{}^c$ is the radiation pattern coefficient. $G_c(\Delta, h)$ is the geometrical spreading factor depending on both epicentral distance Δ and focal depth h. The transfer function $H_m{}^c(\omega)$ for mantle is composed of attenuation factor due to anelasticity. $G_c(\Delta, h)$ and $H_m{}^c(\omega)$ are evaluated using the Jeffreys-Bullen B earth model and MM8–Q_c model by Anderson *et al.* (1965). $H_{cr}{}^c(\omega)$ is the crustal transfer function calculated for the standard model for crust by Fukao (1970), and $H_i(\omega)$ is the impulse response of long period seismograph in WWSSN which is estimated by the use of the Hagiwara's representation (Hagiwara, 1958).

In the case of surface wave, the representation of effective moment can be obtained by the use of the formulation by Ben-Menahem *et al.* (1970) as

$$\begin{aligned} M_e(\omega) &= \frac{\mu\omega G_z(\omega)\,|\,U_z(\omega)/H_i(\omega)\,|}{|\,s_R S_R(\omega) + p_R P_R(\omega) + iq_R Q_R(\omega)\,|} , \quad \text{(for Rayleigh wave)} \\ M_e(\omega) &= \frac{\mu\omega G_\theta(\omega)\,|\,U_\theta(\omega)/H_i(\omega)\,|}{|\,p_L P_L(\omega) + iq_L Q_L(\omega)\,|} , \quad \text{(for Love wave)} \end{aligned} \tag{4}$$

where $U_z(\omega)$ and $U_\theta(\omega)$ are the spectral amplitudes of observed vertical component for Rayleigh waves and transverse component for Love waves, and $G_z(\omega)$ and $G_\theta(\omega)$ are the diminution factors for Rayleigh waves and for Love waves, μ being the rigidity near focal region. Notations of s, p, and q are the factors calculated from source parameters and subscripts of R and L indicate the values for Rayleigh and Love waves respectively. $S(\omega)$, $P(\omega)$ and $Q(\omega)$ are the medium transfer functions. Diminution factors and transfer functions are quoted from the tables by Ben-Menahem *et al.* (1970).

The numerical values of parameters,

$\rho = 3.40\,\mathrm{g/cm^3}$, $V_p = 8.12\,\mathrm{km/sec}$, $V_s = 4.61\,\mathrm{km/sec}$, $\mu = 0.72\times10^{12}\,\mathrm{dyn/cm^2}$,

are adopted in the present computation. The spectrum of observed waves at each station is obtained by FFT program. Seismograms for P and S waves are digitized with a time interval, which is a little different from one seismogram to another within the range of 0.67 and 0.84 sec depending on the enlargement factor of original seismogram. The window is of 200 and 150 sec for P and S waves of the main shock and 50 sec window is adopted for those of other two events.

The sampling rates for surface waves are 4.0 and 4.8 sec for the main and aftershocks in 1975 and the 1974 event respectively. The group velocity window of 3.90 and 3.50 km/sec for the continental path, and 4.10 and 3.50 km/sec for the oceanic path are applied to each trace of Rayleigh waves. For Love waves, the window of 4.30 and 3.90 km/sec for the continental path, and 4.45 and 4.10 km/sec for the oceanic path are adopted.

Examples of spectra thus obtained for P waves at COP are shown in Fig. 9. The azimuthal distribution of observed spectral amplitude of the fundamental mode of Rayleigh waves is seen in Figs. 10, 11 and 12 for the three earthquakes, the period

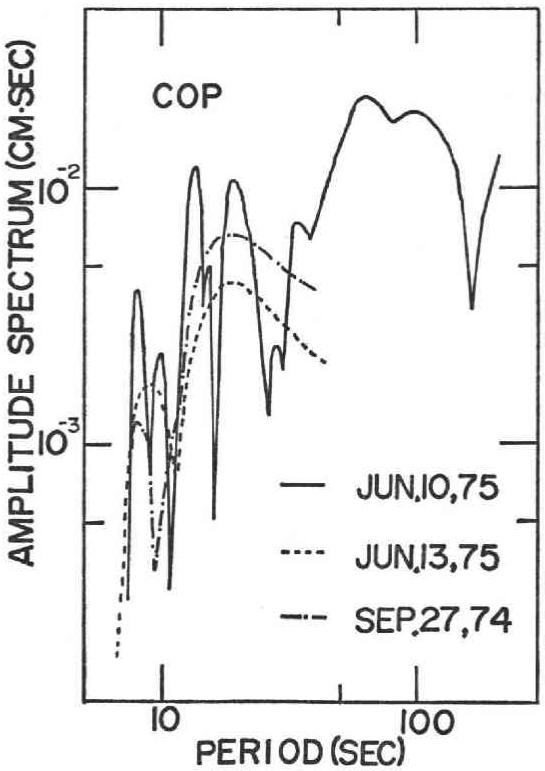

Fig. 9 Spectra of P waves of the three earthquakes at COP, which are deconvolved with instrumental and crustal responses.

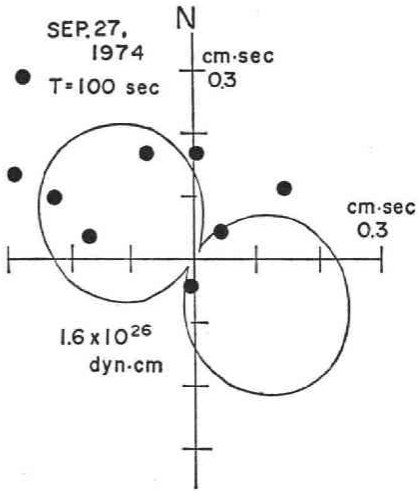

Fig. 10

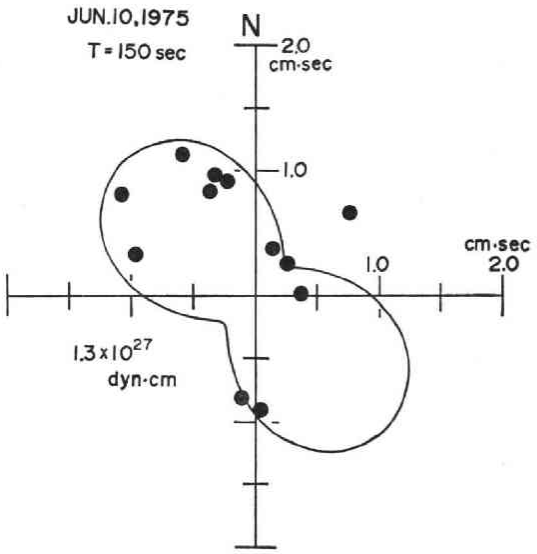

Fig. 11

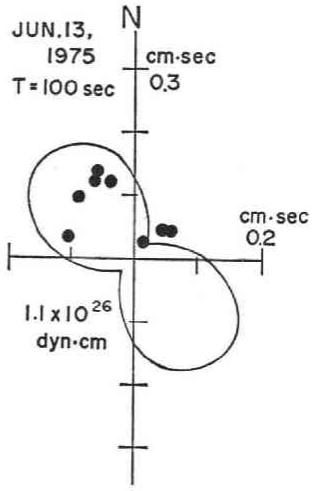

Fig. 12

Fig. 10. Spectral amplitudes of fundamental mode of Rayleigh waves of the 1974 earthquake at 100 sec in period. Solid circles represent observations and solid curve shows theoretical result.

Fig. 11 Spectral amplitudes of fundamental mode of Rayleigh waves of the main shock at 150 sec in period.

Fig. 12 Spectral amplitudes of fundamental mode of Rayleigh waves of the aftershock at 100 sec in period.

in each case being given in the figure. The amplitude in the figure is that deconvolved with the diminution factor so as to represent the value at source region. The theoretically expected pattern is also seen in the figure. For the theoretical calculation the focal mechanism from S waves and effective moment at each period, which is mentioned later, are used. The focal mechanism of the main shock is here assumed to be pure dip slip type, because the dip direction of the fault plane of this earthquake is not so accurately determined, as seen in Table 5. The consistency of observed and theoretical results shown in the figures indicates that the mechanism obtained from S waves is compatible with the observations of not only P waves but also Rayleigh waves for all the three events.

Table 6. The effective moments of the 1974 earthquake

P-wave		Rayleigh wave (R1)			
St.	30(sec)	St.	50	100	150 (sec)
ATU	2.43	ADE	0.965	0.621	3.33
COP	2.26	ATU	1.15	2.45	1.71
ESK	2.78	DAL	1.76	1.09	4.54
KEV	3.04	JCT	0.912	2.77	4.72
MSH	1.95	MAL	0.612	1.28	1.51
		MSH	1.07	1.94	2.38
		NAI	0.827	1.10	0.769
		NAT	2.63	2.01	2.60
		SHI	1.72	1.48	2.39
Average	2.49		1.29	1.64	2.66

(in units of 10^{26} dyn·cm)

Table 8. The effective moments of the aftershock.

P-wave		Rayleigh wave (R1)			
St.	30 (sec)	St.	50	100	150 (sec)
COP	1.34	AAE	0.846	0.732	0.952
GDH	1.16	ALQ	0.992	2.12	3.37
HKC	2.75	ESK	0.568	0.765	0.817
KBS	1.39	IST	0.503	0.568	0.897
KEV	1.56	MAL	0.953	0.850	1.20
NUR	1.89	OXF	3.51	2.37	3.77
VAL	1.85	STU	1.00	0.759	0.711
WES	1.05	WES	2.86	0.660	1.68
Average	1.62		1.40	1.10	1.67

(in units of 10^{26} dyn·cm)

Table 7. The effective moments of the main shock.

P-wave				Rayleigh wave (R1)				SH-wave		Love wave(G1 & G2)	
St.	30	50	70 (sec)	St.	100	150	200 (sec)	St.	70 (sec)	St.	200 (sec)
ATU	1.32	4.80	8.26	AAE	5.97	10.2	12.6	ADE	6.81	ADE	24.4
COP	1.84	5.79	8.67	ADE	8.06	13.0	5.14	GDH	6.11	AKU	15.1
GDH	2.30	4.81	4.67	DAL	18.5	40.8	72.1	PMG	4.18	DAV	18.2 (G2)
KBS	1.94	4.70	10.3	ESK	9.05	11.0	14.6	RIV	4.07	ESK	27.6
KEV	1.08	6.99	7.59	GEO	4.03	5.16	8.22	VAL	6.71	KTG	35.2
KON	1.35	4.55	4.89	IST	9.56	11.6	13.6			MAL	31.3
MSH	1.30	6.37	7.28	MAL	9.68	8.75	11.5			PTO	7.23
NUR	2.53	6.47	7.85	MUN	12.1	10.9	3.76			RIV	13.7
VAL	2.70	5.63	6.60	OXF	16.2	11.6	24.0			STU	24.8
WES	1.96	3.15	4.85	RIV	10.7	11.5	4.46			VAL	11.3
				STU	12.7	11.7	9.59				
				VAL	8.61	10.1	19.7				
Average	1.83	5.33	7.10		10.4	13.0	16.6		5.58		20.9

(in units of 10^{26} dyn·cm)

Since the amplitude spectra are obtained according to the above procedure, the effective moment can be calculated by Eqs. (3) and (4). The effective moments obtained from observations at various stations and for various kinds of waves are listed in Tables 6, 7 and 8 for the three earthquakes. The moments from P and Rayleigh waves are shown *en bloc* in Fig. 13. In the case of the main shock, the small precursory shock is included in the calculation but it does not cause any essential change in the result. Table 7 shows that the moments at 70 and 200 sec from various waves are in fairly good agreement. Fig. 13 represents that the moments for the three events have almost the same value at the period of about 30 sec, but the moment at the period range from 50 to 150 sec for the main shock increases rapidly in spite of that those for the other events are almost constant. The moment at the period of 150 sec for the main shock is about ten times as large as those for the other events.

The seismic moment corresponds to the asymptotic value of effective moment for infinitely long period. They are estimated to be 2.0×10^{26} and 1.4×10^{26} dyn·cm for the 1974 and aftershock respectively as the averages of effective moments between 30 to 150 sec. For the main shock, the asymptotic value cannot be determined from Fig. 13, because the effective moment is still increasing even at 200 sec. However, according to the values of effective moment at 200 sec obtained from Rayleigh and Love waves, it may be safely said that the seismic moment of this event is larger than 2.0×10^{27} dyn·cm probably close to 3.0×10^{27} dyn·cm.

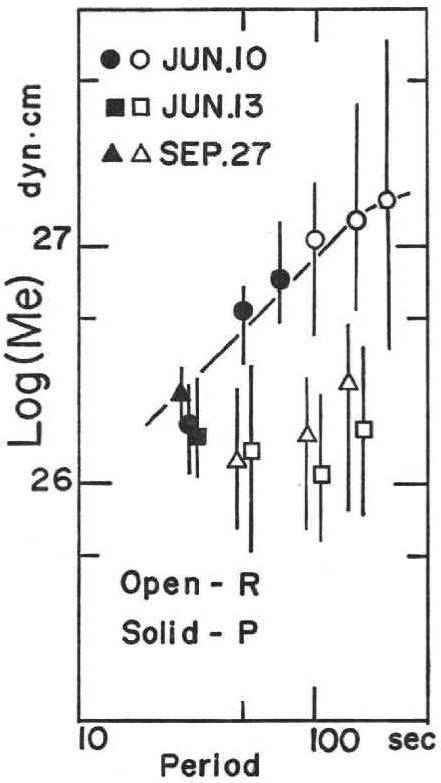

Fig. 13 The effective moments of the three earthquakes from P and Rayleigh waves. The solid and open simbols indicate the values from P and Rayleigh waves. The solid curve represents the theoretical value calculated on the assumption of the seismic moment of 3.0×10^{27} dyn·cm and of the rise time of 50 sec.

The rise time τ of equivalent point source can be obtained under the assumption that the source time function is expressed as

$$M(t,\tau)=M_0(1-\exp(-t/\tau)) \qquad t\geq 0\,, \tag{5}$$

where M_0 is seismic moment. The rise time of the main shock is estimated to be 50 sec if we adopt the seismic moment of 3.0×10^{27} dyn·cm. However, the spectral amplitudes of other two events are almost constant in the period range from 30 to 150 sec as is obvious in Fig. 13. This implies that their moment functions are almost of

the step type, as far as the waves in this period range are concerned. It is concluded, therefore, that the rise time of the main shock is much longer than those of the other two events.

5. Generation of tsunami

Kanamori (1972) stated that an anomalously large tsunami accompanied the earthquake with very long rise time. The excitation of tsunami is essentially related to the long period components of source spectrum (Yamashita and Sato, 1974), while the magnitude is determined from much shorter components. If the rise time is very long, therefore, the tsunami magnitude is expected to be much larger than the formula (1). This type of earthquake is named the "tsunami earthquake" by Kanamori (1972).

This idea is applied to the present case by the use of apparent stress (Aki, 1966 and Wyss, 1970). The apparent stress σ_a is defined as

$$\sigma_a = \mu \frac{E_s}{M_0}, \tag{6}$$

where E_s is the seismic energy, M_0 the seismic moment and μ the rigidity in focal region. E_s can be calculated by the Gutenberg and Richter's relation

$$\log E_s = 1.5\,M + 11.8, \tag{7}$$

from magnitude M. It is expected that the tsunami earthquake would have smaller apparent stress than that of ordinary earthquake. We adopt JMA magnitude and seismic moment obtained in the previous section and assume the rigidity μ of 0.72×10^{12} dyn/cm^2. Table 9 shows the apparent stress thus obtained, as well as those of major earthquakes along the trench, one exception being the Niigata Earthquake in 1964 occurring near the Japan Sea coast. This table indicates that the Sanriku Earthquake in 1896, which was accompanied with anomalously large tsunami, and the present main shock give very small apparent stresses compared to other earthquakes. The value of 3.0×10^{27} dyn·cm is taken in this calculation as the seismic moment of the

Table 9. Earthquake and tsunami magnitudes, seismic moments and apparent stresses of major earthquakes in and near Japan.

No.	Date(J.M.T.)	Epicenter	Location	M (JMA)	m*	σ_a (bar)	Mo ($\times10^{27}$dyn·cm)	
1.	1896 Jun. 15	39.6°N 144.2°E	Sanriku	7.6	3.0	2.3	50	(Kanamori 1972)
2.	1933 Mar. 3	39.1° 144.7°	Sanriku	8.3	3.0	29.8	43	(Kanamori 1972)
3.	1963 Oct. 13	43°45′ 149°58′	Kurile	8.1	2.0	8.6	75	(Kanamori 1970)
4.	1964 Jun. 16	38°21′ 139°11′	Niigata	7.5	2.0	26.9	3	(Aki 1966)
5.	1968 Jan. 29	43°11′ 147°00′	Kurile	6.9	0.0	—	—	
6.	1968 May.16	40°44′ 143°35′	Sanriku	7.9	2.0	11.5	28	(Kanamori 1971)
7.	1969 Aug. 12	42°42′ 147°37′	Kurile	7.8	2.0	10.3	22	(Abe 1973)
8.	1973 Jun. 17	42°58′ 145°57′	Off Nemuro	7.4	1.5	8.5	6.7	(Shimazaki 1974)
9.	1974 Sep. 27	42°45′ 146°40′	Kurile	6.6	−1.0	18.0	0.20	(This study)
10.	1975 Jun. 10	42°46′ 147°13′	Kurile	7.0	1.5	4.8	3	(This study)
11.	1975 Jun. 13	42°54′ 147°30′	Kurile	6.5	—	18.0	0.14	(This study)

*m: tsunami magnitude according to Hatori (1969, 1971, 1975)

main shock, but even if we take the smallest possible value of 2.0×10^{27} dyn·cm instead, the above conclusion remains the same. Consequently the present main shock is concluded to be one of tsunami earthquakes.

Yamashita and Sato (1974) indicated that the generation of tsunami is considerably influenced by the dip angle of the fault and focal depth, based on the calculation for the case of pure dip slip fault. The main shock in the present study has a smaller dip angle than the other two events and the difference in excitation of tsunami cannot be attributed to the effect of dip angle. The focal depths of the main and aftershocks are about 15 km as seen in Table 1, whereas that of the 1974 event is approximately 45 km. According to Yamashita and Sato's result the difference in focal depth affects the generation of tsunami by the factor of not more than two. On the other hand, the difference of tsunami in the present case is approximately one of the order of magnitude. The difference in focal depth, therefore, should not be the main cause of the difference in tsunami generation.

6. Discussions

We will discuss about two features of the main shock in this section. One is the long rise time of equivalent point source and the other is the long wave train with large amplitude after initial P wave motion.

The source spectrum was discussed by the use of double couple point source model in the previous section and the anomalously long rise time was obtained about the main shock. This may be affected by both the effects of source finiteness and rise time of dislocation in actual source but it is not obvious which effect is more strong. If the rise time τ of point source is regarded as the total time interval of rupture of whole fault, it is roughly expressed as

$$\tau = \frac{L}{v} + \tau_0 , \tag{8}$$

where L is fault length, v is rupture velocity, and τ_0 is the rise time of dislocation. In the case of the main shock, τ is obtained to be 50 sec in §4 and L is determined to be about 50 km from the aftershock area represented in Fig. 2. Then, on the assumption that the dislocation function is a step type ($\tau_0=0$), rupture velocity v is calculated from Eq. (8) to be 1 km/sec, which is anomalously small in comparison with the average value for earthquakes in this region. To the contrary, if v is assumed to be 3 km/sec, which is the common value, the rise time of dislocation is obtained to be about 30 sec. This is again anomalously long. Therefore, it is natural to consider that the long rise time may be due to both comparatively slow rupture velocity and long rise time of dislocation.

As stated previously, the P wave form of the main shock on June 10, 1975 exhibits a complicated feature. The seismograms at the station of GDH in Fig. 14 represents an example of long wave train with large amplitude after initial P wave motion. The duration time of the train is about 200 sec and the maximum amplitude

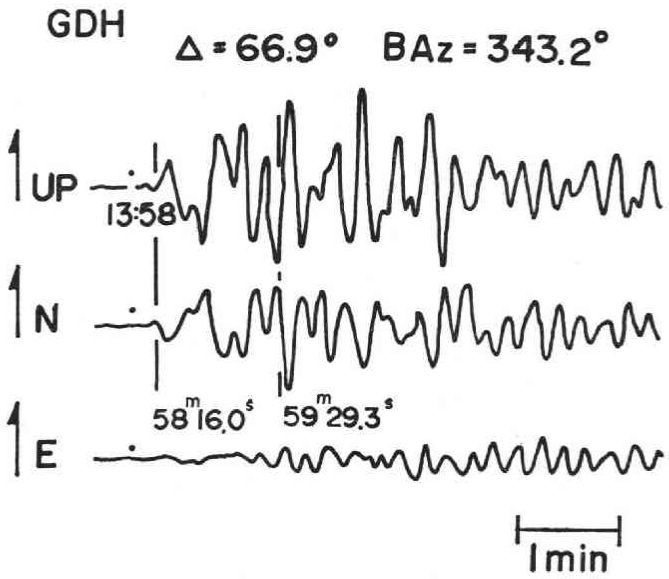

Fig. 14 Seismograms in three components of the main shock at GDH.

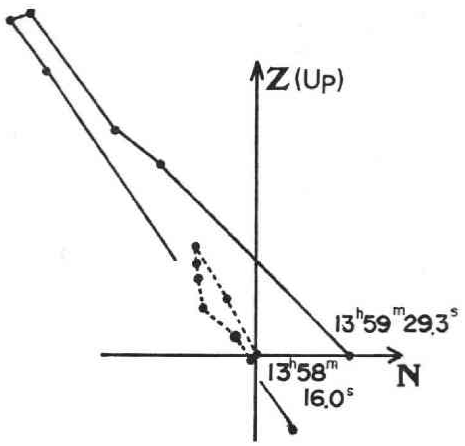

Fig. 15 The particle motions in Z-N plane of initial P phase and a later phase, of which arrival times are indicated on the seismograms of GDH in Fig. 14. Each phase is digitized with a time interval of 1.3 sec.

of later wave is larger than that of initial P. The particle motion of initial wave is compared with that of a part of later wave train in Fig. 15. The comparison shows clearly that the particle motion is similar to each other. Other part of the train also shows the similar feature. The later part, therefore, is reasonably considered to consist mainly of compressional waves with nearly the same incident angle as initial motion.

Seismograms at the stations in almost the same azimuth are represented in Fig. 16 in order of epicentral distance. This figure shows evidently that peaks and troughs in various stations correspond fairly well with a constant time difference from P

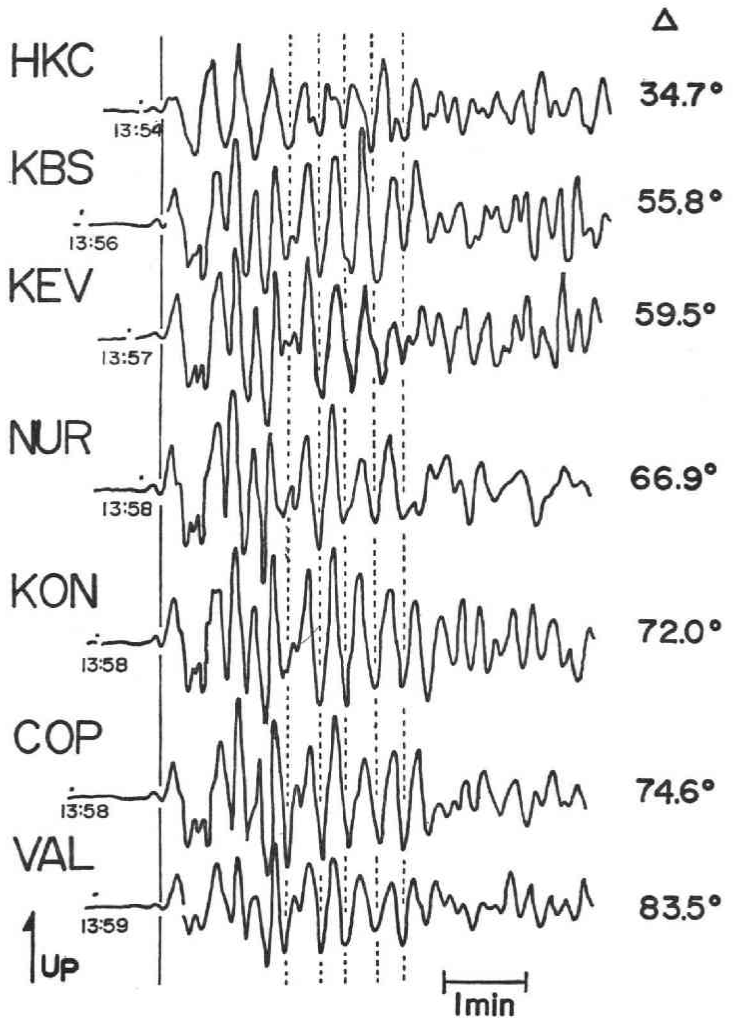

Fig. 16 Seismograms in vertical component of the main shock arranged in order of epicentral distance. Solid line indicates the onset of main fracture.

irrespective of epicentral distance. This implies that these waves have the same travel path as that of initial P. These facts suggest that the excitation of these waves should be attributed to some origin near focal region.

However the later waves have some different features from initial motion. Fig. 17 illustrates the seismograms arranged in order of station azimuth. The amplitudes of later phases at COR, ADE and RIV are roughly equivalent to those at other stations, although these stations are situated near the nodal plane of P waves so that initial motions are small in amplitude. Furthermore, the polarity of later wave is not always consistent with that of initial motion as seen in Fig. 17.

The source spectra are calculated based on the seismograms at COR and KEV as seen in Fig. 18. The former station is very close to the nodal plane of P while the latter

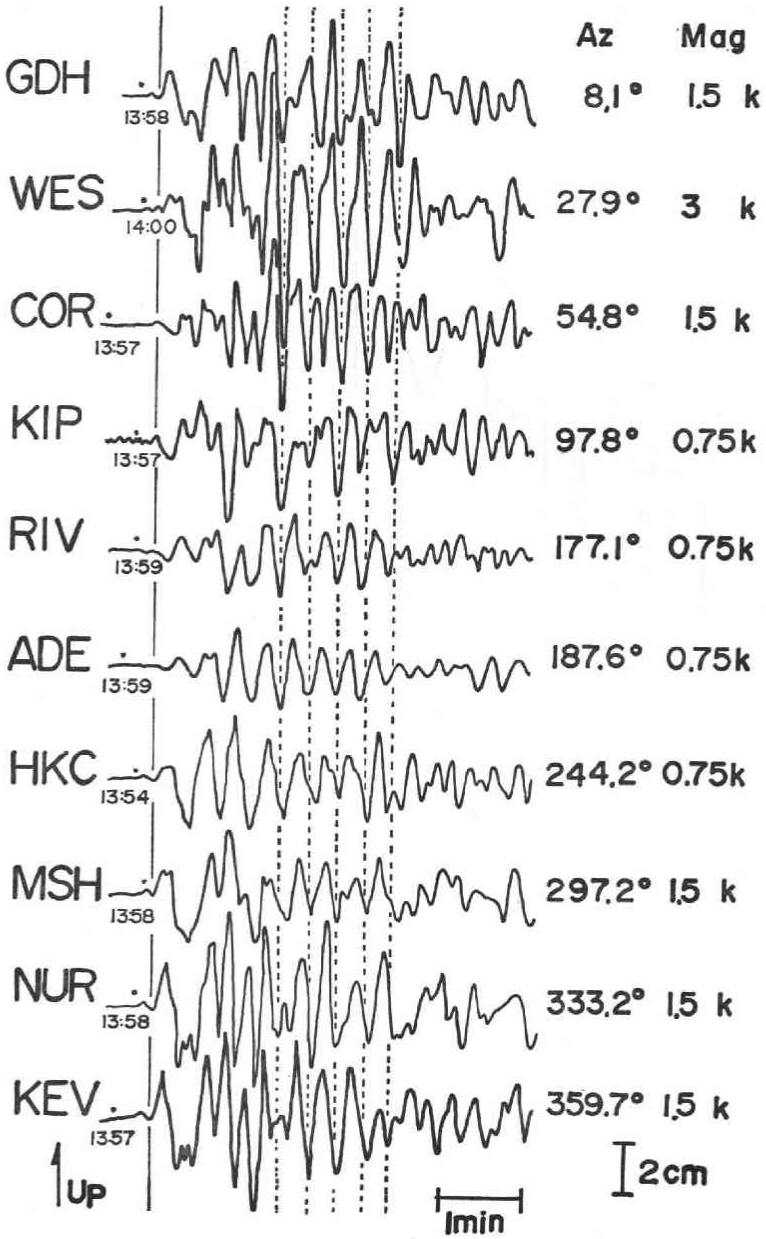

Fig. 17 Seismograms of the main shock arranged in order of station azimuth. Mag means magnification of seismometer. Other symbols are the same as in Fig. 16.

is far from that, and the spectrum from COR record contains much influence of later waves, whereas that from KEV consists mainly of initial P wave. These curves are deconvolved with instrumental and crustal responses. As seen in the figure the spectral amplitude for COR record is much smaller in the period range longer than 50 sec compared to that for KEV. Big peaks in spectrum from 10 to 20 sec are seen with similar

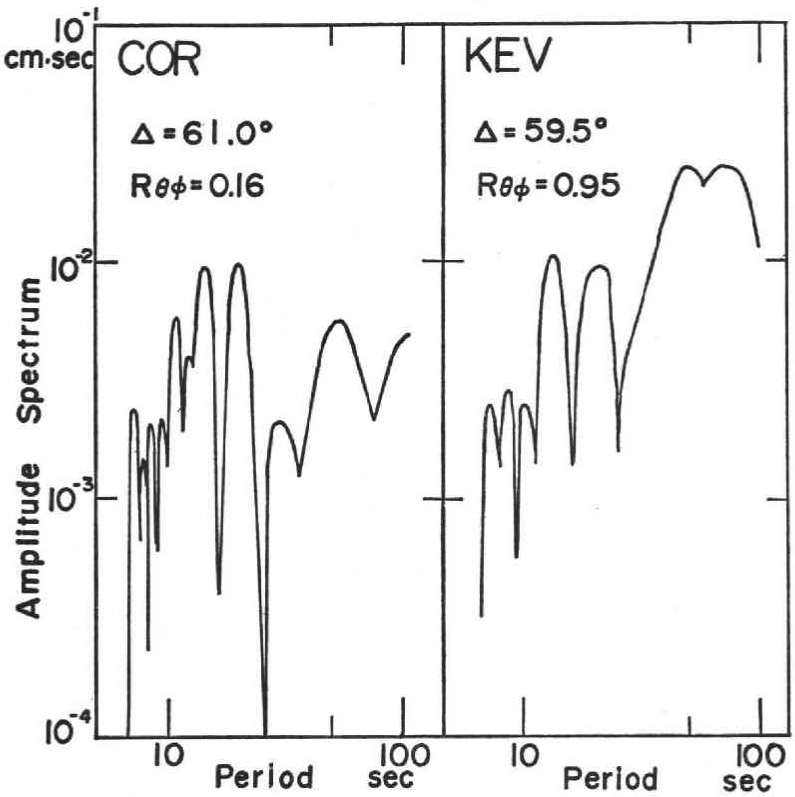

Fig. 18 Comparison of source spectra obtained from P wave trains in vertical component of the main shock at COR and KEV within 200 sec from the onset. These are deconvolved with instrumental and crustal responses. $R_{\theta\phi}$ is the radiation coefficient of P waves.

magnitude of amplitude in both cases. This indicates that the later waves have a predominant component at the period range from 10 to 20 sec. In the calculation of source spectra and moments in the previous section, the peaks at 10 and 20 sec were ignored for this reason.

The generation of these later waves may be due to the multiple reflection of waves near the focal region. One of the reasons of this idea is that the later waves have a predominant period and time intervals between P and later arrivals are almost constant. It is an impotant problem to study whether the later phases with large amplitude are only in this particular case or rather common in other cases of great and shallow earthquakes.

7. Conclusions

The main results obtained from this study are breifly summarized as follows:

(1) The epicenter of the main shock was located near the trenchward edge of the aftershock area. This is a contrary feature to that in usual cases of major earthquakes along the trench.

(2) The focal mechanism solution determined from the S wave data satisfies sufficiently well the observations of P and Rayleigh waves in every case.

(3) The focal mechanism solutions of all of the three earthquakes are thrust type.

(4) A small precursory event took place about 10 seconds before the main fracture of the main shock. The mechanism solution of the precursor is similar to that of the main fracture.

(5) The dip angle of the fault plane of the main shock is smaller than those of other two earthquakes by about ten degrees. This may be compatible with the fact that its epicenter is much closer to the trench than those of other two.

(6) The source spectra obtained from body and surface waves indicate that the rise time of equivalent point source is much longer for the main shock than those of other two earthquakes. The seismic moments for the three earthquakes are calculated to be 2.0×10^{26}, 3.0×10^{27} and 1.4×10^{26} dyn·cm for the 1974, the main and aftershock, although their magnitudes are not so much different from one another.

(7) The main shock gives very small apparent stress compared with other major earthquakes along the Japan and Kurile trench. This fact indicates that the main shock can be classified as the tsunami earthquake with very long rise time. This is the reason why the main shock excited an anomalously large tsunami compared with the other two cases.

Acknowledgements: We wish express our thanks to Prof. T. Hirasawa for reading the manuscript critically and his instructive suggestions during the course of this study. We are indebted to Drs. K. Yamamoto and H. Oda for their helpful discussions.

References

Abe, K., 1973: Tsunami and mechanism of great earthquakes, Phys. Earth Planet. Interiors, **7**, 143–153.

Aki, K., 1966: Generation and propagation of G-waves from the Niigata earthquake of June 16, 1964. Part 2, Bull. Earthq. Res. Inst., **44**, 73–88.

Anderson, D.L., A. Ben-Menahem, and C.B. Archambeau, 1965: Attenuation of seismic energy in the upper mantle, J. Geophys. Res., **70**, 1441–1448.

Ben-Menahem, A., and M.N. Toksöz, 1963: Source mechanism from spectra of long period seismic surface waves. 2. The Kamchatka earthquake of November 4, 1952, J. Geophys. Res., **68**, 5207–5222.

Ben-Menahem, A., M. Rosenman and D.G. Harkrider, 1970: Fast evaluation of source parameters from isolated surface wave signals. Part 1. Universal tables, Bull. Seism. Soc. Am., **60**, 1337–1387.

Fukao, Y., 1970: Focal process of a deep focus earthquake as deduced from long period P and S waves, Bull. Earthq. Res. Inst., **48**, 707–727.

Hagiwara, T., 1958: A note on the theory of the electomagnetic seismograph, Bull. Earthq. Res. Inst., **36**, 139–164.

Haskell, N.A., 1953: The dispersion of surface waves on multilayered media, Bull. Seism. Soc. Am., **43**, 17–34.

Hatori, T., 1969: Dimensions and geographic distribution of tsunami source near Japan, Bull. Earthq. Res. Inst., **47**, 185–214.

Hatori, T., 1970: An investigation of the tsunami generated by the east Hokkaido earthquake of August, 1969, Bull. Earthq. Res. Inst., **48**, 399–412.

Hatori, T., 1971: Tsunami sources in Hokkaido and southern Kurile regions, Bull. Earthq. Res. Inst., **49**, 63–75.

Hatori, T., 1975: Tsunami activity in eastern Hokkaido after the off Nemuro peninsula earthquake in 1973 (in Japanese), Zisin, Ser. 2, **28**, 461–471.

Hirasawa, T., and W. Stauder, 1965: On the seismic body waves from a finite moving source, Bull. Seism. Soc. Am., **55**, 237–262.

Hirasawa, T., 1966: A least squares method for the focal mechanism determination from S wave data, Bull. Earthq. Res. Inst., **44**, 901–938.

Horiuchi, S., J. Koyama, Y. Izutani, I. Onodera, and H. Hirasawa, 1976: Earthquake generating stress in the Kurile-Kamchatka seismic region derived from superposition of P-wave initial motions, Sci. Rep. Tôhoku Univ., Ser. 5, **23**, 67–81.

Iida, K., 1958: Magnitude and energy of earthquakes accompanied by tsunami, and tsunami energy, J. Earth Science, Nagoya Univ., **6**, 101–112.

Kanamori, H., 1970: Synthesis of long period surface waves and its application to earthquake source studies – Kurile Islands earthquake of October 13, 1963, J. Geophys. Res., **75**, 5011–5027.

Kanamori, H., 1971: Focal mechanism of the Tokachi-oki earthquake of May 16, 1968· Contortion of the lithosphere at a junction of two trenches, Tectonophysics, **12**, 1–13.

Kanamori, H., 1972: Mechanism of tsunami earthquakes, Phys. Earth Planet. Interiors, **5**, 346–359.

Kanamori, H. and D.L., Anderson, 1975: Theoretical basis of some empirical relation in seismology, Bull. Seism. Soc. Am., **65**, 1073–1095.

Kelleher, J., L. Sykes, and J. Oliver, 1973: Possible critera for predicting earthquake locations and their application to major plate boundaries of the Pacific and the Caribbean, J. Geophys. Res, **78**, 2547–2585.

Koyama, J., 1976: Source process of the Vladivostok deep focus earthquake of September 10, 1973, Sci. Rep. Tôhoku Univ., Ser. 5, **23**, 83–101.

Koyama, J., 1977: Seismic moment of the Vladivostok deep focus earthquake of September 29, 1973 deduced from P-waves and mantle Rayleigh waves, Phys. Earth Planet· Interiors (in press).

Nuttli, O., and J.D. Whitmore, 1962: On the determination of the polarization angle of the S wave, Bull. Seism. Soc. Am., **52**, 95–107.

Shimazaki, K., 1974: Nemuro-oki earthquake of June 17, 1973: a lithospheric rebound at the upper half of the interface, Phys. Earth Planet. Interiors, **9**, 314–327.

Shimazaki, K., and R.J. Geller, 1977: Source process of the Kurile islands tsunami earthquake of June 10, 1975 (abstract), EOS, **58**, 446.

Stauder, W., and L. Mualchin, 1976: Fault motion in the larger earthquakes of Kurile-Kamchatka arc and the Kurile- Hokkaido corner, J. Geophys. Res., **81**, 297–308.

Yamashita, T., and R. Sato, 1974: Generation of tsunami by a fault model, J. Phys. Earth, **22**, 415–440.

Yamashita, T., and R. Sato 1976: Correlation of tsunami and sub-oceanic Rayleigh wave amplitudes possibility of the use of Rayleigh wave in tsunami warning system, J. Phys. Earth, **24**, 397–416.

Wyss, M, 1970: Stress estimates of South America shallow and deep earthquakes, J. Geophys Res. **75**, 1529–1544.